Small teams of myosin Vc motors coordinate their stepping for efficient cargo transport on actin bundles

Received for publication, February 9, 2017, and in revised form, May 3, 2017 Published, Papers in Press, May 5, 2017, DOI 10.1074/jbc.M117.780791

Elena B. Krementsova[‡1], Ken'ya Furuta[§1], Kazuhiro Oiwa[§], Kathleen M. Trybus[‡2], and M. Yusuf Ali[‡3]

From the [‡]Department of Molecular Physiology and Biophysics, University of Vermont, Burlington, Vermont 05405 and the [§]Advanced ICT Research Institute, National Institute of Information and Communications Technology, Kobe 651-2492, Japan

Edited by Velia M. Fowler

Myosin Vc (myoVc) is unique among vertebrate class V myosin isoforms in that it requires teams of motors to move continuously on single actin filaments. Single molecules of myoVc cannot take multiple hand-over-hand steps from one actin-binding site to the next without dissociating, in stark contrast to the well studied myosin Va (myoVa) isoform. At low salt, single myoVc motors can, however, move processively on actin bundles, and at physiologic ionic strength, even teams of myoVc motors require actin bundles to sustain continuous motion. Here, we linked defined numbers of myoVc or myoVa molecules to DNA nanostructures as synthetic cargos. Using total internal reflectance fluorescence microscopy, we compared the stepping behavior of myoVc *versus* myoVa ensembles and myoVc stepping patterns on single actin filaments *versus* actin bundles. Run lengths of both myoVc and myoVa teams increased with motor number, but only multiple myoVc motors showed a run-length enhancement on actin bundles compared with actin filaments. By resolving the stepping behavior of individual myoVc motors with a quantum dot bound to the motor domain, we found that coupling of two myoVc motors significantly decreased the futile back and side steps that were frequently observed for single myoVc motors. Changes in the inter-motor distance between two coupled myoVc motors affected stepping dynamics, suggesting that mechanical tension coordinates the stepping behavior of two myoVc motors for efficient directional motion. Our study provides a molecular basis to explain how teams of myoVc motors are suited to transport cargos such as zymogen granules on actin bundles.

In vertebrates, three class V myosin isoforms transport intracellular cargoes such as melanosomes, secretory vesicles, endoplasmic reticulum, and mRNA on actin tracks. Myosin Va (myoVa)[4] is the most well characterized isoform and the prototype of a processive myosin, *i.e.* a single motor that can take many steps on an actin filament without dissociating (1). More limited assays with myosin Vb suggested that it is also processive (2). In contrast, myosin Vc, which is predominantly expressed in glandular tissues such as pancreas, colon, and stomach, was the only vertebrate class V isoform to be kinetically characterized as non-processive, implying that it would be unable to move cargo continuously as a single motor (2–4). This observation was surprising because myoVc is known to be involved in transport of secretory vesicles to the apical membrane (4). It was recently shown that in the exocrine pancreas, parallel bundles of actin filaments nucleated by formins at the plasma membrane are the tracks on which zymogen granules are trafficked (5). Consistent with this biological observation, we recently showed that actin bundles are the required track for small ensembles of myoVc, attached to a quantum dot, to continuously move at physiologic ionic strength (150 mM KCl) (6). The number of motors attached to the Qdot was not defined, nor was the stepping pattern of motors in the ensemble followed. The preference for bundles is related to the observation that a single myoVc takes ~40% back steps and lateral steps under unloaded conditions, and it has a very broad turning angle distribution compared with the highly processive myoVa motor, suggesting that only the additional binding sites provided by an actin bundle allow continuous motion. Chimeric constructs further identified the lever arm/rod domains of myoVc as the structural elements responsible for this unusual stepping behavior. When the myoVc motor domain was fused to the lever arm/rod of myoVa, it exhibited no back steps and moved processively on single actin filaments, similar to myoVa (6).

The requirement for teams of myoVc to move continuously on actin bundles near physiologic ionic strength prompted us to more closely investigate the behavior of two coupled myoVc motors. Sakamoto and co-workers (7) showed for the first time that when two myoVc motors were coupled via a DNA scaffold, the complex moved continuously at low ionic strength even on single actin filaments. In that study, the movement of the labeled scaffold was tracked, so that the stepping patterns of individual myoVc heads in the ensemble could not be moni-

This work was supported by American Heart Association Grant 12SDG11930002 (to M. Y. A.), Grant-in-aid for Scientific Research, Japan, 15KT0155 (to K. F.), and National Institutes of Health Grant GM078097 (to K. M. T.). The authors declare that they have no conflicts of interest with the contents of this article. The content is solely the responsibility of the authors and does not necessarily represent the official views of the National Institutes of Health.

[1] Both authors contributed equally to this work.

[2] To whom correspondence may be addressed: Dept. of Molecular Physiology and Biophysics, Health Science Research Facility 132, University of Vermont, Burlington, VT 05405. Tel.: 802-656-8750; E-mail: kathleen.trybus@uvm.edu.

[3] To whom correspondence may be addressed: Dept. of Molecular Physiology and Biophysics, Health Science Research Facility 131, University of Vermont, Burlington, VT 05405. Tel.: 802-656-9513; Fax: 802-656-0747; E-mail: yusuf.ali@med.uvm.edu.

[4] The abbreviations used are: myoVa, myosin Va; myoVc, myosin Vc; Qdots, quantum dots; TIRF, total internal reflectance fluorescence; TRITC, tetramethylrhodamine isothiocyanate; ANOVA, analysis of variance.

tored. The requirement for actin bundles for myoVc ensembles was not observed because experiments were performed solely at low salt conditions. Nonetheless, this study established that two motors increased the probability of at least one myoVc head remaining bound to the filament at any given time. Numerous studies have shown that intracellular cargos are transported by the coordination of multiple motors. Melanosomes, for example, are associated with as many as 60 myoVa motors *in vivo*, although it is likely that only a subset of this number is actively engaged with the track at any given time (8). The mechanism by which the mechanical properties of individual motors contribute to or share their collective transport duties depends on the particular motor or motors involved (8). A number of studies have predicted the collective behavior of motor ensembles transporting a common cargo, but the number of motors and their stepping pattern were generally unknown (9–11). In neither of the previous studies with myoVc ensembles (6, 7) was the stepping dynamics of individual heads in the ensemble followed.

Here, we designed DNA origamis or DNA scaffolds to act as a synthetic cargo for linking a defined number of Qdot-labeled myoVc motors with defined inter-motor spacing (12, 13). This approach allowed us to follow the stepping dynamics of two myoVc motors on actin filaments and actin bundles and to compare this behavior with myoVa. We confirmed that a single molecule of myoVc walks on an actin bundle with frequent back and side steps, and we further showed that coupling two myoVc motors significantly decreases the frequency of such futile steps and causes both the leading and trailing motors to coordinate. Run-length enhancement by multiple myoVc motors is significantly higher on actin bundles than on actin filaments, in contrast to multiple processive myoVa motors, which show a greater run-length enhancement with motor number on single actin filaments. This study provides a molecular basis to explain how multiple myoVc motors are optimized to move large exocrine secretory granules on actin bundles in the final stages of secretion (5).

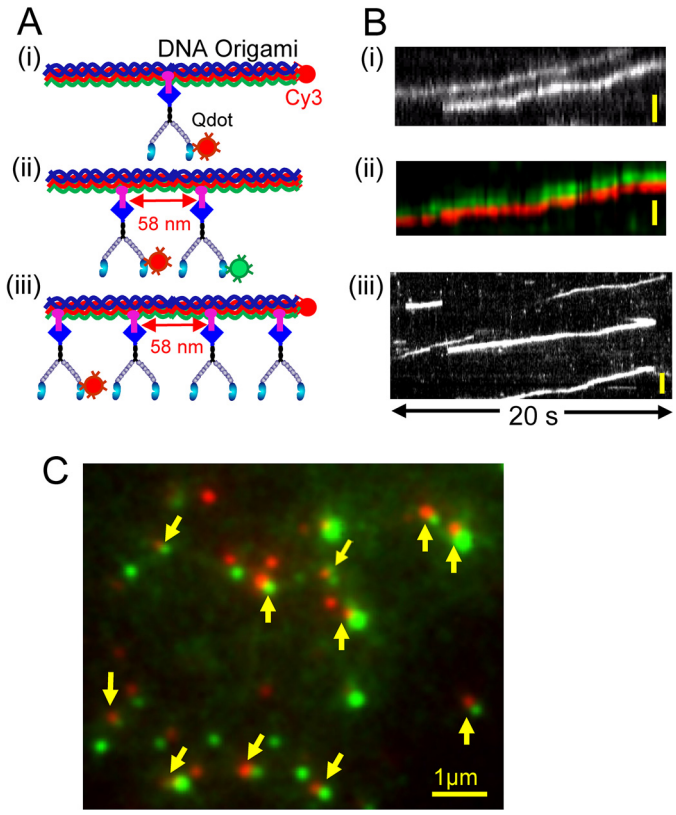

Figure 1. Experimental design to visualize motility of small ensembles of myosin. *A,* 1, 2, or 4 myosin motors containing a SNAP tag at the C terminus of the myosin heavy chain (*blue diamond*) are bound to a DNA origami containing varying numbers of SNAP ligands. Single and 4-motor complexes were visualized using Qdots or Cy3 (*red circle*) attached to the DNA origami. In the 2-motor complex, one motor domain of each of the two molecules was labeled with a different colored Qdot (*red* or *green*). *B, panel i,* representative kymographs of a single motor moving on an TRITC-labeled actin bundle (not shown); *panel ii,* 2-motor complex (*red* and *green*) moving on an unlabeled actin filament. The images for red and green Qdots were not corrected for color registration errors in this figure for visual purposes. *Panel iii,* 4-motor complex moving along a TRITC (not shown)-labeled actin bundle at 1 mM MgATP. *Scale bar,* 1 μm. Elapsed times are indicated. *C,* data showing that two different colored motors (*red* and *green* Qdots and *yellow arrows*) can be efficiently coupled to the 2-motor DNA origami. The images for *red* and *green* Qdots were separated from each other because these images were obtained through different light paths. The images (*red* and *green* Qdots) were not corrected for such mapping errors for visual purposes. *Scale bar,* 1 μm.

Results

Comparison of movement by small ensembles of myoVc versus myoVa on actin filaments

Here we used DNA nanostructures as synthetic cargos for linking defined numbers of myosin molecules. An advantage of the DNA origami nanotube is that its rigidity keeps the average attachment spacing between the motors constant during movement (12). The motion of a single motor, or small ensembles of myoVc or myoVa, was observed by coupling motors to a DNA origami containing one, two, or four SNAP ligands (Fig. 1*A*). To establish that the motion of the motor is not affected by attachment to the DNA origami, a single processive myoVa motor was attached to a DNA nanotube that contained one binding site. A quantum dot (Qdot) was used to label one of the two motor domains (see "Experimental procedures"). The motion of motor-origami complexes on single actin filaments, immobilized onto the glass surface, was observed using a total internal reflectance fluorescence (TIRF) microscope with high temporal (33–100 ms) and spatial resolution (6 nm). A single myoVa bound to the origami moved processively for 0.8 ± 0.12 μm ($n = 67$) at an average velocity of 378 ± 94 nm/s ($n = 67$), similar to our previous observations using myoVa not attached to DNA (14). A single molecule of myoVc did not move processively on single actin filaments, whether or not it was coupled to the origami.

Run length of motors was determined from an exponential decay distribution function and reported as means and standard error of the fit (mean ± S.E.). To determine statistical significance between two sets of run lengths or step lifetimes, the Kolmogorov-Smirnov test was used. For comparison of multiple run lengths, a Kruskal-Wallis test with Dunn's multiple comparisons test was performed. Velocity was measured from the fit to a Gaussian distribution function and are reported as mean and standard deviation (mean ± S.D.). To determine statistical significance between two velocity or step size distributions, the unpaired *t* test was used. For the statisti-

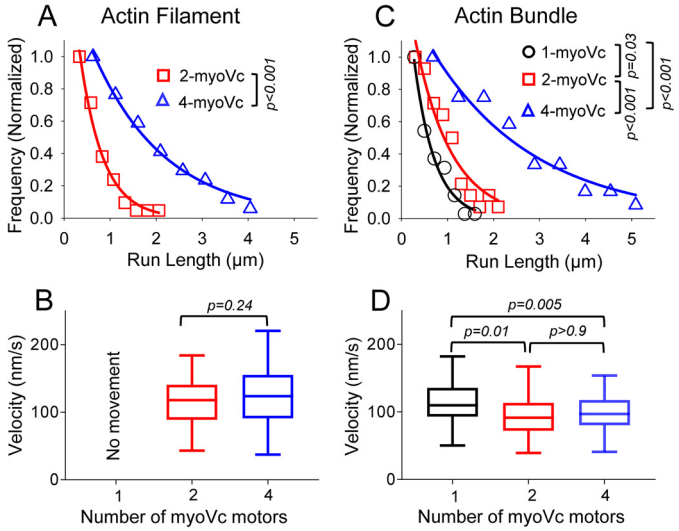

Figure 2. Effect of myoVc motor number on run length and velocity on actin filaments and bundles. See Table 1 for run length and velocity values. *p* values are indicated on the *graphs*. *A,* on single actin filaments, the run length of the 4-myoVc complex increased significantly compared with the 2-myoVc complex. *B,* velocity of the 2-myoVc and 4-myoVc complex was the same on single actin filaments. *C,* on actin bundles, myoVc run-length increased significantly with motor number. *D,* velocity of 2- or 4-myoVc motor complexes was reduced significantly compared with a single motor on bundles, but the velocity of the 2 *versus* 4-myoVc complex was the same. The velocity of the 2-myoVc and 4-myoVc complex was reduced by 25% and 20% compared with a single motor. Run-length values are mean ± S.E., and velocity values are mean ± S.D. Conditions: 25 mM imidazole, pH 7.4, 4 mM $MgCl_2$, 1 mM EGTA, 25 mM KCl, 10 mM DTT.

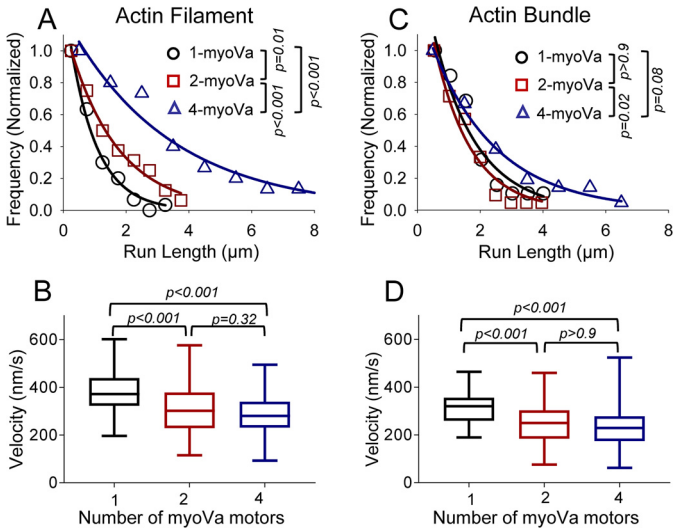

Figure 3. Effect of myoVa motor number on run length and velocity on actin filaments and bundles. See Table 1 for run length and velocity values. *p* values are indicated on the *graphs*. *A,* on single actin filaments, the run length of myoVa increased significantly as a function of motor number. The run length of the 2- and 4-myoVa complex on actin filaments was 1.8- and 3.9-fold longer, respectively, than that of a single myoVa. *B,* velocity of 2- or 4-myoVa motor complexes was reduced significantly compared with a single motor on single actin filaments. Velocity for the 2- *versus* 4-myoVa complex was not significantly different. *C,* on actin bundles, the run length of the 2-myoVa complex of myoVa was unchanged but increased significantly for the 4-myoVa complex compared with a single motor. *D,* velocity of 2- or 4-myoVa motor complexes was reduced significantly compared with a single motor on actin bundles. Conditions: 25 mM imidazole, pH 7.4, 4 mM $MgCl_2$, 1 mM EGTA, 25 mM KCl, 10 mM DTT.

cal analysis of multiple sets of velocity data, ANOVA with Bonferroni multiple comparisons test was performed.

For the 2-myoVc complex bound to the DNA origami, one motor was labeled on its motor domain with a red Qdot (emits at 655 nm), and the other motor was labeled with a green Qdot on its motor domain (emits at 565 nm) (Fig. 1*A*). Motion on TRITC-labeled or unlabeled actin filaments was observed. This labeling strategy allowed us to directly track the stepping dynamics of each of the two motors in the ensemble during motion. In contrast to a single myoVc motor, two myoVc motors bound to a DNA nanotube moved continuously on single actin filaments at 1 mM MgATP and 25 mM KCl (Fig. 1*B*). We observed that 40% (n = 165) of complexes were labeled with dual color Qdots (Fig. 1*C*). Given that statistically a maximum of 50% of the DNA origamis could be dual color (equimolar red and green motors), the binding affinity of myoVc motors to the origami and labeling with Qdots must both be very efficient (80%) (Fig. 1*C*; see "Experimental procedures"). For the 4-ligand DNA origami, a 5-fold molar excess of motor over SNAP-ligand was used to favor full occupancy. Binomial statistics showed that on average there will be 3.6 motors per origami (see "Experimental procedures"). The 4-motor complex was tracked by labeling a subset of the motors with a red Qdot (emits 655 nm) or Cy3 attached to the DNA origami.

On single actin filaments, the run length of myoVc increased 2.9-fold from 2 to 4 motors but the velocity remained unchanged (Fig. 2, *A* and *B,* and Table 1). Similarly, the run length of myoVa increased significantly with motor number (Fig. 3*A*). The velocity of both the 2- and 4-motor myoVa complex was, however, reduced significantly compared with a single motor (Fig. 3*B* and Table 1). Multiple myoVc motors thus work efficiently in ensembles by showing longer run lengths without a loss of speed on actin filaments at low ionic strength (Fig. 2, *A* and *B*). At any given motor number, run lengths on single actin filaments were significantly longer for myoVa than myoVc (Table 1). Although the run lengths of the 2- and 4-motor complex of myoVc were 0.52 ± 0.06 μm (n = 56) and 1.5 ± 0.24 μm (n = 58), these values were 1.4 ± 0.21 (n = 54) and 3.1 ± 0.4 (n = 56) for myoVa (p = 0.001 for 2-motor complexes and p = 0.01 for 4-motor complexes).

Comparison of movement of small ensembles of myoVc versus myoVa on actin bundles

Consistent with bundles being a processivity factor for myoVc (2), single myoVc motors can take multiple steps on actin bundles at 25 mM KCl (Fig. 1, *A* and *B*). The average run length of a single myoVc molecule on actin bundles was 0.40 ± 0.07 μm (n = 85), and the velocity was 116 ± 38 nm/s (n = 85) (Fig. 2, *C* and *D*, and Table 1). The run lengths of 2-myoVc and 4-myoVc motors complexes were 2.2- and 5.3-fold longer than that of a single motor (Fig. 2*C* and Table 1). In contrast, the run length of myoVa was unchanged for the 2- and 4-motor complex compared with a single motor (Fig. 3*C* and Table 1). However, the run length of 4-motor complex was increased 1.8-fold (p = 0.02) compared with a 2-motor complex (Fig. 3*C*).

For myoVc, the velocity of the 2-and 4-myoVc complex was significantly reduced by 25% and 20% compared with a single motor (Fig. 2*D* and Table 1). Similarly, velocities of myoVa ensembles were significantly slower than single motors (Fig. 3*D*

Table 1

Comparison of run length and velocity on actin bundles *versus* actin filaments

Run length values were obtained by fitting the exponential decay function, and the standard error (S.E.) values are errors of the fit. Velocity values were reported as mean ± S.D.) obtained from the gaussian distribution. The indicated *p* values are a comparison between actin bundles and actin filaments at a fixed motor number for a given myosin isoform. At any given motor number, run lengths on single actin filaments were significantly longer for myoVa than myoVc ($p = 0.001$ for 2-motor complexes, $p = 0.01$ for 4-motor complexes). For statistical significance between two sets of velocity data, an unpaired *t* test with 95% confidence interval was performed. For run length, the Kolmogorov-Smirnov test with 95% confidence interval was used.

		Run length (μm)			Velocity (nm/s)		
Motor	Track	Single motor	Two motors	Four motors	Single motor	Two motors	Four motors
myoVc	Actin filament	No movement	0.52 ± 0.06 ($n = 56$)	1.5 ± 0.24 ($n = 58$)	No movement	117 ± 40 ($n = 56$)	125 ± 46 ($n = 58$)
	Actin bundle	0.4 ± 0.07 ($n = 85$)	0.86 ± 0.17 ($n = 62$)	2.1 ± 0.36 ($n = 50$)	116 ± 38 ($n = 85$)	87 ± 31 ($n = 62$)	93 ± 29 ($n = 50$)
			$p = 0.05$	$p = 0.04$		$p = 0.001$	$p < 0.001$
myoVa	Actin filament	0.8 ± 0.12 ($n = 67$)	1.4 ± 0.21 ($n = 54$)	3.1 ± 0.4 ($n = 56$)	378 ± 94 ($n = 67$)	290 ± 116 ($n = 54$)	272 ± 95 ($n = 56$)
	Actin bundle	1.4 ± 0.33 ($n = 63$)	1.2 ± 0.28 ($n = 59$)	2.2 ± 0.26 ($n = 52$)	308 ± 72 ($n = 63$)	239 ± 96 ($n = 59$)	231 ± 86 ($n = 52$)
		$p < 0.001$	$p = 0.64$	$p = 0.08$	$p < 0.001$	$p < 0.001$	$p = 0.02$

and Table 1), similar to the reduction observed in previous studies in which two myoVa motors were linked via a DNA scaffold or a Qdot (14, 15). On actin bundles, multiple myoVc motors work efficiently in ensembles by showing longer run lengths, although at the expense of a lower speed.

Comparison of motion of myoVc and myoVa on actin bundles versus actin filaments

Comparing motor performance on single actin filaments *versus* bundles, myoVc and myoVa also differed. Although a single myoVc motor is non-processive on a single actin filament, it can take multiple steps on actin bundles at low ionic strength (Fig. 2*C* and Table 1). For both 2- and 4-myoVc complexes, the run length on bundles was significantly longer than on single actin filaments (Fig. 2, *A* and *C,* and Table 1). These run-length data are consistent with the idea that myoVc ensembles are specialized for cargo transport on actin cables (6).

The run length of a single myoVa motor on an actin bundle is significantly higher than on an actin filament, but the velocity is slower (Fig. 3, *A* and *C,* and Table 1). In contrast, the run lengths of 2- and 4-myoVa complexes on actin bundles were not statistically different from that on single actin filaments (Fig. 3, *A* and *C,* and Table 1). Irrespective of motor number for both myoVc and myoVa, the velocity on actin bundles is significantly slower than on an actin filament (Table 1).

MyoVc movement at physiologic ionic strength

Consistently, the multimotor myoVc complexes coupled to the DNA origami could not move continuously on single actin filaments at 150 mM KCl but showed continuous motion on actin bundles, with a run length of 0.39 ± 0.06 μm ($n = 64$) for the 2-myoVc complex and 1.3 ± 0.3 μm ($n = 58$) for the 4-myoVc complex (Fig. 4*A*). This result implies that both multiple myoVc motors and actin bundles are required for transporting secretory vesicles in the cell (4, 5).

The run length of the 2- and 4-motor complexes was significantly lower ($p < 0.001$; $p < 0.001$) at 150 mM KCl compared with what was observed at 25 mM KCl (Fig. 2*C versus* 4*A*). At 150 mM KCl, the velocity of the 2-motor complex (120 ± 47 nm/s, $n = 64$) was 28% higher ($p = <0.001$) than at 25 mM KCl (87 ± 31, $n = 62$), but the velocity of the 4-motor complex was not significantly different at the two salt concentrations (109 ± 46 nm/s, $n = 58$ at 150 mM KCl; 93 ± 29 nm/s, $n = 50$ at 25 mM KCl; $p = 0.06$) (Fig. 2*D versus* 4*B*).

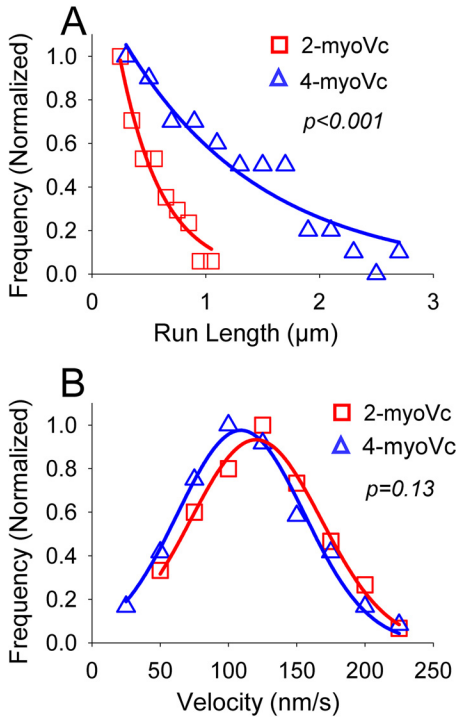

Figure 4. Run length and velocity of myoVc at physiologic salt concentration. *A,* at 150 mM KCl, the run length of a 4-myoVc complex (1.3 ± 0.3 μm, $n = 58$) on actin bundles was 3.3-fold longer than that of a 2-myoVc complex (0.39 ± 0.06 μm, $n = 64$). *p* values are indicated on the *graph*. *B,* velocity of the 2-myoVc complex on actin bundles was not significantly different from that of a 4-myoVc complex (120 ± 47 nm/s, $n = 64$ *versus* 109 ± 46 nm/s, $n = 58$). *p* values are indicated on the graph. Conditions: 25 mM imidazole, pH 7.4, 4 mM $MgCl_2$, 1 mM EGTA, 150 mM KCl, 10 mM DTT.

Cargo rigidity affects run length of myoVc

We compared myoVc motion when coupled to a DNA scaffold *versus* a DNA origami (Fig. 5*A*). The DNA scaffold consisted of one double-stranded DNA and is less stiff than the DNA origami that was constructed from six double DNA strands. We attached two myoVc, each with a different color Qdot on a motor domain, to either a DNA scaffold or a DNA origami, and we measured the distance between the two labeled heads (Fig. 5*A*). The distance between two motors on the DNA origami (57 ± 42 nm) was the same as the spacing between the binding sites (58 nm). However, the distance between two motors on the scaffold was 48 ± 31 nm, smaller than the spacing between binding sites (63 nm). These results are consistent with the scaffold being more flexible than the origami.

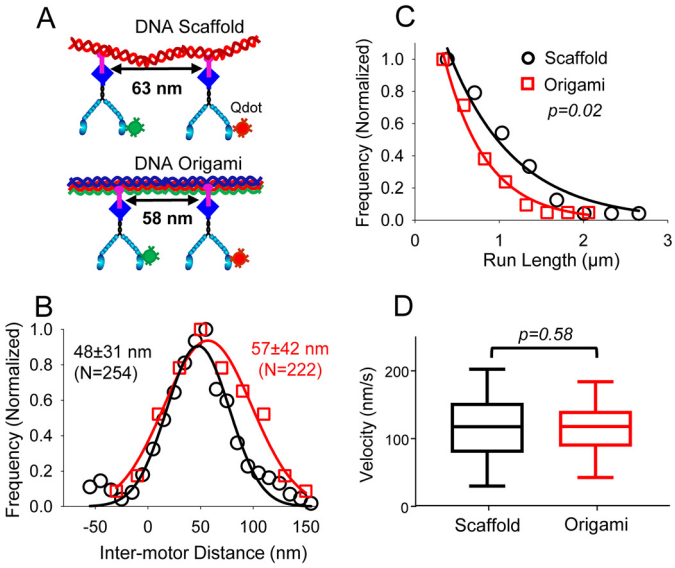

Figure 5. Effect of cargo rigidity. *A,* illustration of a flexible DNA scaffold and a rigid DNA origami with 63- or 58-nm spacing (repeated from Fig. 1*A, panel ii*), respectively. Motors with a C-terminal SNAP tag were conjugated to a DNA scaffold or DNA origami containing SNAP ligand. *B,* distance between two labeled heads of myoVc linked to the DNA scaffold (*black*) or DNA origami (*red*). *C,* run length of the 2-motor complex (0.52 ± 0.06, $n = 56$) attached to the DNA origami is significantly lower ($p = 0.02$) than when the complex is attached to the DNA scaffold (0.8 ± 0.18 μm, $n = 72$). *D,* velocity of the 2-motor complex (117 ± 40, $n = 56$) attached to the DNA origami (*red*) is not significantly different from the complex attached to the DNA scaffold (119 ± 55 nm/s, $n = 72$, $p = 0.58$)). Conditions: 25 mM imidazole, pH 7.4, 4 mM $MgCl_2$, 1 mM EGTA, 25 mM KCl, 10 mM DTT.

For comparing how synthetic cargo flexibility affected velocity and run length on single actin filaments, myoVc was only labeled with a red Qdot (emits 655 nm) (see "Experimental procedures"). Because a single myoVc cannot move on actin filaments, moving complexes by definition had two myoVc motors bound. The run length of two motors attached to a flexible DNA scaffold is significantly higher (0.8 ± 0.18 μm, $n = 72$) than when they are attached to the rigid DNA origami (0.52 ± 0.06, $n = 56$, $p = 0.02$) (Fig. 5*C*), suggesting that cargo rigidity may also play an important role in coordinating myoVc motors. The velocity was unchanged when 2-myoVc motors were attached to the scaffold *versus* origami (Fig. 5*D*).

Two myoVc motors promote directional movement on actin bundles

The movement of a single myoVc *versus* a 2-myoVc complex was compared on actin bundles. The single myoVc had one motor domain labeled with a Qdot. For the 2-myoVc complex separated by 58 nm on a DNA origami, one motor domain of each myoVc was labeled with a different colored Qdot to allow unambiguous monitoring of the stepping dynamics of each motor (Fig. 1*A*). To examine the stepping dynamics at high temporal and spatial resolution, the MgATP concentration was reduced to 2 μM to slow the stepping speed. A single myoVc was unable to move straight, switching between filaments in the bundle with almost every step (Fig. 6*A*). In addition to lateral steps, myoVc took a large number of back steps (24%) on the actin bundle (Fig. 6, *B* and *C*). Steps of myoVc motors were identified by a step-finding program (14), and step sizes were determined from the fit of a Gaussian distribution function. The mean forward step size of myoVc on the actin bundle was 63 ± 26 nm ($n = 67$) (Fig. 6*C*), the same as the step size of myoVa (63 ± 26 nm, $n = 142$) (14). The backward step size of myoVc on actin bundles (51 ± 22 nm, $n = 21$) was significantly shorter ($p < 0.001$) than that of the forward step size (Fig. 6*C*).

Remarkably, the 2-myoVc complex moved much more directionally than a single motor (Fig. 6*D*). The directional movement of a single and 2-myoVc complex was quantified by measuring the turning angle between successive steps as done previously (6, 16) (Fig. 6*D, inset*). The stepping pattern of a single myoVc motor showed that there is no bias in turning one direction over the other, as determined from the *x*-*y* position (Fig. 6, *A* and *D*, *inset*). For single motors, 54% of the unbound heads landed on the left side of the bound head, and the other 46% landed on the right side. Similarly, for the 2-myoVc complex, 53% of the unbound heads landed on the left side of the bound head, and 47% landed on the right side. The average turning angle of a single (−2.4 ± 76°, mean ± S.D., $n = 100$) *versus* a 2-myoVc complex (0.31 ± 29°, mean ± S.D., $n = 64$) was determined from the fit to a Gaussian distribution function. The smaller standard deviation (S.D.) of the 2-myoVc complex indicates that it moved more directionally than a single motor.

The step-sizes of both leading (68 ± 25 nm, $n = 60$) and trailing (60 ± 28 nm, $n = 55$) motors of the 2-myoVc complex were not significantly different from that of a single motor ($p = 0.49$ and $p = 0.75$), but the frequency of the back steps was greatly reduced when 2-myoVc were physically linked (Fig. 6, *B* and *E*). Although the back step frequency of a single motor was 24%, it was only ~8% for both leading and trailing motors within the 2-myoVc complex (Fig. 6, *C* and *F*). The directional transport with reduced frequency of back steps or side steps suggests that myoVc motors cooperate to transport cargo along actin bundles.

Forward and backward steps of two coupled myoVc motors on single actin filaments

To further understand how multiple myoVc motors coordinate during cargo transport, the stepping dynamics of each Qdot-labeled motor within a 2-myoVc complex, coupled to a DNA origami with 58-nm inter-motor distance, was monitored on single actin filaments at low ionic strength (Fig. 7*A*). The mean step sizes of the leading (66 ± 27 nm, $n = 95$; Fig. 7*B, green*) and trailing motors (61 ± 24 nm, $n = 101$; Fig. 7*B, red*) within the complex were not significantly different from a single motor stepping on an actin bundle (63 ± 26 nm, $n = 67$) ($p = 0.24$; $p = 0.34$) (Fig. 6*C*). The mean backward step-size of both the leading (60 ± 19 nm, $n = 11$) and the trailing (56 ± 20 nm, $n = 10$) motors were slightly shorter ($p = 0.026$; $p = 0.007$) than that of the forward steps (Fig. 7*B*). In addition to forward steps, both the leading and trailing motors take a similar number of back steps (10 and 9%), similar to the back step frequency of the 2-myoVc complex moving on actin bundles (~8%) (Fig. 6*F*). These values are lower than the 24% backsteps seen with a single myoVc motor (Fig. 6*C*) and show that coupling two motors reduces backsteps. In contrast, when two processive myoVa motors were linked via a Qdot, the leading motor took a higher number of back steps (11%) than the trailing motor (3%) (14).

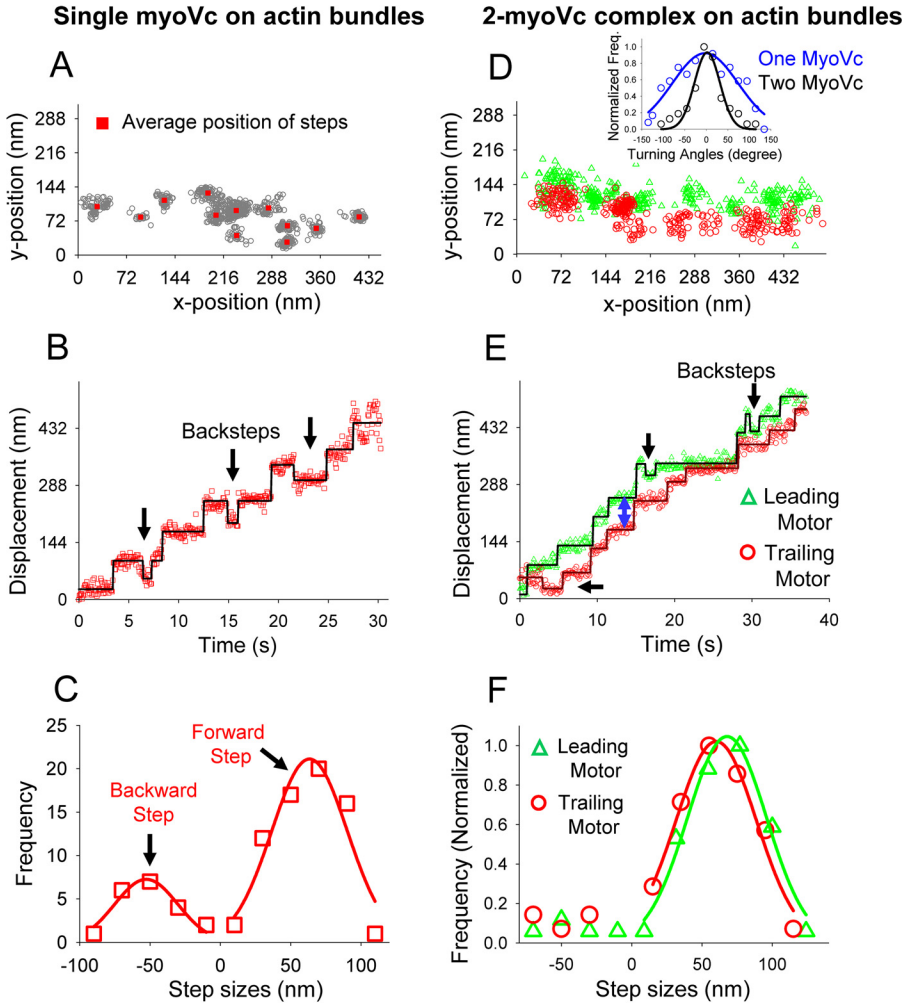

Figure 6. Motion of one *versus* two myoVc motors on actin bundles at 2 μM MgATP. *A–C*, stepping dynamics of a single myoVc motor. *A, x,y* trajectory (*gray* circles) of a single myoVc where the average position of each step is indicated by *red squares*. *B*, representative displacement *versus* time trajectory showed that a single myoVc motor moves on actin bundles in a stepwise manner but with a significant number of back steps (*arrows*). *C*, mean forward 63 ± 26 nm (mean ± S.D., $n = 67$) and backward step sizes (51 ± 22 nm, mean ± S.D., $n = 21$) were determined from the fit of single Gaussian function. *D–F*, stepping dynamics of a 2-myoVc motor complex, in which one myoVc is labeled with a *red* Qdot and the other with a *green* Qdot. *D, x,y* trajectory of the leading (*green*) and trailing (*red*) motor within the 2-motor complex. *Inset*, histogram comparing the turning angles of a single motor (*blue*) with the 2-motor complex (*black*). The average turning angles of a single and 2-motor complex were −2.4 ± 76° (mean ± S.D.) and 0.31 ± 29° (mean ± S.D.), respectively. *E*, representative trajectory showed that the leading (*green*) and trailing (*red*) motors within the complex moved on actin bundles in a stepwise manner. While stepping on the actin bundle, the inter-motor distance (*blue arrow*) fluctuates. The leading motor took an occasional back step (*black arrow*). *F*, forward and backward step-size distributions of the leading motor (*green triangles*) and the trailing motor (*red circles*). Conditions: 25 mM imidazole, pH 7.4, 4 mM $MgCl_2$, 1 mM EGTA, 25 mM KCl, 10 mM DTT.

The step lifetimes of the leading and trailing motors were plotted in histograms and fitted with $P(t) = tk^2e^{-kt}$ (see "Experimental procedures"). Because both the leading and trailing motors are physically linked, the average step lifetime of both motors should be the same. As expected, the forward step lifetimes of the leading (3.3 ± 0.4s, $n = 132$) and the trailing (3.1 ± 0.5s, $n = 133$) motors are not significantly different ($p = 0.87$) (Fig. 7*C*). Similarly, the backward step lifetimes of both the leading and the trailing motors are the same (leading motor, 1.1 ± 0.2 s, $n = 15$; trailing motor, 1.2 ± 0.3 s, $n = 14$) ($p = 0.45$) (Fig. 7*D*).

Inter-motor distance

While moving on an actin track or actin bundles, the distance between the two coupled myoVc motors fluctuates (Fig. 6*E*, 7*A*), despite being attached to the DNA origami with a 58-nm inter-motor spacing (17). The distance between two labeled heads of the leading and trailing motors (Figs. 6*E* and 7*A*, *blue arrows*) was measured from the displacement *versus* time traces. As expected, the average distance between motors was 57 ± 42 nm ($n = 277$; mean ± S.D.) on actin filaments (Fig. 8*B*, *red*). When moving on actin bundles, the inter-motor distance between two labeled heads of myoVc was 53 ± 33 nm, mean ± S.D. ($n = 313$) (Fig. 8*B*, *blue*). Because of the flexibility between the lever arm and rod domain, and the linkage between the origami and motor, the inter-motor distances fluctuated from −36 to ~160 nm (Fig. 8*B*). A negative inter-motor distance was occasionally seen when the trailing motor passed the leading motor at the beginning of the run (Fig. 7*A*, *pink arrow*) or when the trailing motor detached and reattached to the filament in front of the leading motor.

Stepping rate and delay time between steps

To examine whether myoVc motors coordinate their steps when mechanically coupled through a DNA origami, or

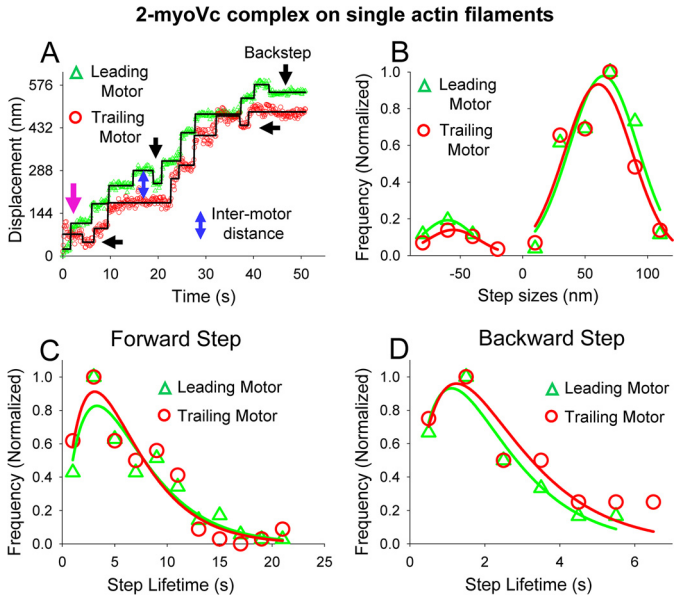

Figure 7. Characterization of a 2-myoVc complex stepping on single actin filaments. *A,* representative displacement *versus* time trajectory showed the stepwise movement of the leading (*green*) and trailing motor (*red*) of two myoVc complexes on an actin filament at 2 μM MgATP. While stepping, the distance between the two labeled heads fluctuates (*blue double-headed arrow*). *B,* step size distribution of the leading (*green triangles*) and the trailing motor (*red squares*) within a complex. The mean step sizes of the leading and the trailing motors were 66 ± 27 nm (n = 95, *green*) and 61 ± 28 nm (n = 101, *red*), respectively. Both leading and trailing motors take ~9% back steps. The forward (*C*) and backward (*D*) step lifetime distributions of the leading and trailing motors were the same. Conditions: 25 mM imidazole, pH 7.4, 4 mM $MgCl_2$, 1 mM EGTA, 25 mM KCl, 10 mM DTT.

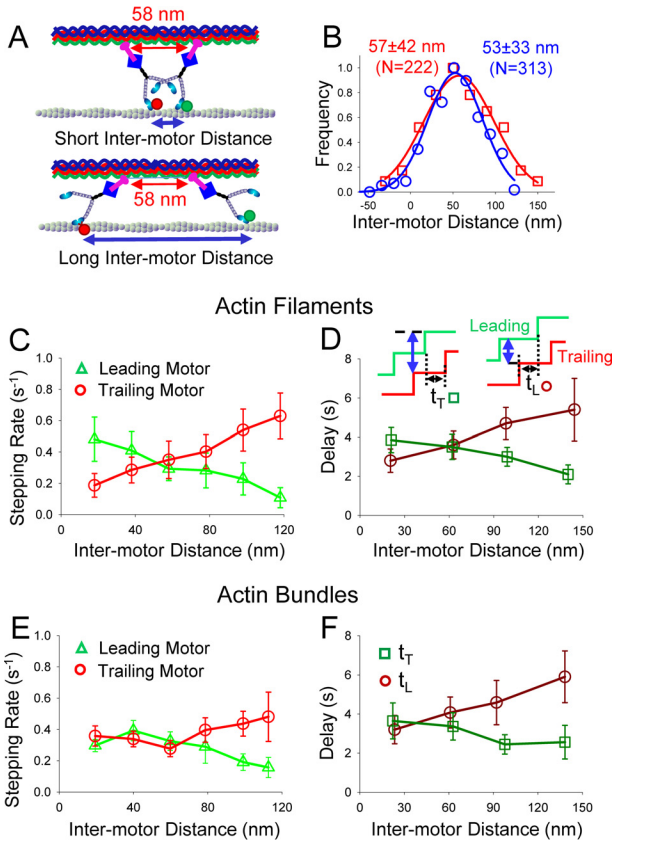

Figure 8. Characterization of inter-motor distances during myoVc stepping. *A,* illustration of a 2-motor complex showing the fluctuation of inter-motor distances on a single actin filament. *B,* distance between the labeled heads can fluctuate from −40 to 160 nm, with a mean distance of 57 ± 42 nm (mean ± S.D., n = 222) on actin filament (*red*) and 53 ± 33 nm (mean ± S.D., n = 313) on actin bundle (*blue*). For comparison, this *graph* (*red*) was repeated from Fig. 5*B*. *C,* stepping rate of leading (*green triangles*) and trailing (*red circles*) myoVc motors as a function of inter-motor distance on actin filaments. *D,* delay time between steps of the leading and the trailing motors on an actin filament. The average time delay (t_T) (*dark green squares*) between a forward step of the leading motor and the next forward step of the trailing motor was plotted as a function of the inter-motor distance (*blue arrow*). These time delays were measured immediately after the step of the leading motor (*dark green squares*). Similarly, time delay (t_L) indicates the average time (*dark red circles*) between a step of the trailing motor and the next step of the leading motor. *E* and *F,* similar stepping rate and delay time as in *C* and *D*, but on actin bundles. Conditions: 25 mM imidazole, pH 7.4, 4 mM $MgCl_2$, 1 mM EGTA, 25 mM KCl, 10 mM DTT.

whether they move independently during transport (14, 18, 19), the stepping rate was measured as a function of inter-motor distance (Fig. 8*C*). The average stepping rate of the leading and trailing motor must be similar because both motors are physically linked. The stepping rate of both the leading and trailing motors are similar at an inter-motor distance of 58 ± 20 nm on an actin filament (Fig. 8*C*). As the distance between motors increased further (>78 nm), the stepping rate of the leading motor decreased sharply, in contrast to the stepping rate of the trailing motor, which increased. The opposite effect was observed at short inter-motor distance (<38 nm) where the leading motor's stepping rate is higher than that of the trailing motor. This may be due to compression in the linkage between motors and/or a competition by the two motors for binding sites on the actin filament.

On actin bundles, the stepping rates of the leading and trailing motors are the same at inter-motor distances from 20 to 80 nm. At inter-motor distance of >80 nm, the stepping rate of the trailing motor increased, and the leading head increased as a function of inter-motor distance (Fig. 8*E*). In contrast to the behavior seen on an actin filament, the stepping rate of the leading motor is the same as the trailing motor at short inter-motor distances on actin bundles. This difference might occur when motors within the complex walk on parallel actin filaments in the actin bundle. Therefore, the chance of competing for a binding site will be much less than what we observed on an actin filament. The stepping rate results suggest that as the inter-motor distance grows, leading motors tend to be pulled backward leading to their slowing, whereas trailing motors tend to be pulled forward leading to an increased stepping rate. Because the stepping rate changes as a function of inter-motor distance, the leading and trailing motors mechanically impact each other and are not independent.

To further understand how the steps of the leading and trailing motors are coordinated, we measured the time delay (t_T) for the trailing motor to take its step just after a step of the leading motor on actin filaments and actin bundles (Fig. 8, *D* and *F*) (14). Interestingly, t_T is reduced as inter-motor distance is increased, suggesting that the trailing motor begins to coordinate its steps with that of the leading motor. The time delay for the leading motor to take a step just after the trailing motor (t_L) increased with inter-motor distance, suggesting that the leading motor also coordinates with the trailing motor (Fig. 8, *D* and *F*). The variation of these two time delays (t_T and t_L) indicates that the degree of coordination changes with the distance between motors, both on single filaments and on bundles.

These delay time and stepping rate relationships as a function of inter-motor distance suggest that the leading and trailing motors mechanically interact under tension. Overall, these results are similar to our recent observations with myoVa, except that t_L was unaffected by inter-motor distance when myoVa walked on actin filaments (14).

Discussion

Here we compared the motion of two and four myoVc motors, coupled via a DNA origami as surrogate cargo, with that of a single myoVc motor. Our results suggest that myoVc has unique attributes that specialize it for working in ensembles to move cargo on actin bundles. We confirmed that a single myoVc is a non-processive motor on an actin filament but that it can take multiple steps on actin bundles at low ionic strength (6). Actin bundles act as a "processivity factor" because the unbound head of myoVc switched filaments with almost every step, and thus the additional binding sites for the head in the bundle significantly reduce the termination probability of the motor. In contrast to the behavior of a single motor, coupling two myoVc motors via a common cargo produced continuous, unidirectional movement. Our labeling strategy furthermore allowed us to follow the stepping dynamics of one motor domain of each of the two coupled myoVc molecules, with high spatial and temporal resolution. Remarkably, the 2-myoVc complex essentially abolished the back steps and lateral steps taken by a single myoVc on an actin bundle. A potential mechanism is that because motors are mechanically coupled under tension, one motor can prevent the other from taking back steps or lateral steps. A similar mechanism was suggested for mammalian dynein. Whereas a single dynein motor in the absence of its native activators (dynactin and cargo adaptors such as BicD) exhibits diffusional movement (20), coupling two dynein motors decreased the frequency of backward motion and favored directed transport along the microtubule (17). In cells, it is typical for multiple motors to work together to transport intracellular cargo, but in the case of myoVc multiple motor transport appears to be a necessity (18, 21–23).

Bundle preference

The preference of myoVc for actin bundles is evidenced by the observations that a single myoVc motor requires bundles to move processively at low ionic strength and even small ensembles of myoVc require bundles to move continuously near physiologic ionic strength. Our previous work showed that elements in the lever arm/rod of myoVc were responsible for the large number of back steps that myoVc takes (6). The junction between the lever arm and rod of myoVc may be extremely flexible and cause an unfavorable geometry between the unbound head and the next binding site on a single actin filament, but allow forward motion on actin bundles which provides additional lateral binding sites for myoVc motors. The step size of myoVc is also shorter (66 ± 27 nm) than the helical pitch of the actin filament, in contrast to processive myoVa whose step size of 72 ± 12 nm on actin filaments more closely matches the helical pitch of the actin filament. Therefore, the lateral steps of myoVc may also result from the structural mismatch between the step size of myoVc and available actin-binding sites. If the unbound head cannot bind to the next binding site on the same filament, it could bind to the adjacent filament within a bundle and thus prevent detachment.

A single myoVc transitions from being non-processive on single filaments to processive on bundles, but the 2- and 4-myoVc complexes also show longer run lengths on bundles compared with filaments. This property may be an adaptation to help restrict the activity of myoVc to specialized actin cables, such as those assembled during the final stages of secretion in the exocrine pancreas (5). In contrast, 2- or 4-motor complexes of the processive myoVa isoform show shorter run lengths on bundles than on single actin filaments. It is possible that myoVa experiences an off-axis resistive load on an actin bundle, which results in a higher termination rate from the track. The myoVa was shown to be sensitive when an off-axis resistive load was applied by an optical trap in a particular direction (24), but this property was not tested for myoVc.

Run lengths of small ensembles

Run lengths of 2- and 4-motors complexes of myoVc are lower than for myoVa (Table 1). We previously showed that each processive myoVa motor within a 2-motor complex coordinates to move continuously on a single actin filament. Remarkably, a 2-motor complex of myoVa is driven by single motor for ~50% of the time (14, 15). When one of two myoVa motors detaches from the actin filament, the other attached motor is still capable of taking multiple steps on an actin filament. The detached motor can rebind and continue processive movement (14).

Single molecules of myoVc, in contrast, cannot move processively on single actin filaments, and thus when one motor within the 2-myoVc complex detaches, the second motor simultaneously detaches. Therefore, it is expected that the run length of 2- or 4-motor complexes of myoVc will be shorter than that of myoVa, as observed.

MyoVc molecules coordinate to transport cargo

Modeling and experimental studies suggested that if motors are independent of each other, the velocity will remain the same, and the run length will increase greatly compared with a single motor (18, 25, 26). Our results showed that the velocity of the 2-myoVc complex was reduced by 25%, and the run length increased ~2-fold, compared with a single myoVc, suggesting that the 2 motors are mechanically coupled under tension. Similar results were obtained when two processive myoVa motors were physically linked using a Qdot or a DNA scaffold (14, 15). Our result is consistent with the observation that motors can negatively interfere with each other during motion (19).

The mechanical interaction between two coupled motors also depends on the stiffness of the cargo and properties of the motor (15, 27, 28). Here we showed that two myoVc motors have longer run lengths when coupled via a flexible DNA linker compared with a rigid linker. Future studies with motors bound to liposomes, which more closely mimic cellular cargo, will provide further insight into the effect of cargo stiffness on motion, although the strict control of motor number is lost with this approach (27).

Because two motors are physically linked, it is expected that when the leading motor experiences a resistive load by the trailing motor, the trailing motor would also experience an assistive load by the leading motor. This result is supported by our observation that the stepping rate of the leading myoVc motor decreased rapidly at a higher inter-motor distance, whereas the stepping rate of the trailing motor increased. Similar results were obtained when the 2-myoVc complex moved on actin bundles. Thus, both the leading and trailing myoVc motors coordinate with each other and remain mechanically coupled under tension during cargo transport. This behavior is similar to what we observed for myoVa (14). Both processive and non-processive motors thus apply some common mechanisms related to inter-motor coordination.

The leading and trailing heads of pairs of myoVa *versus* myoVc show some differences. Normally, myoVa takes back steps only when it experiences a resistive load (29). When 2-myoVa motors were linked via a Qdot, the leading myoVa took a higher number of back steps than the trailing motor (11% *versus* 3%), indicating that the leading motor is sensitive to the resistive load applied by the trailing motor (14). Optical trapping studies also showed that myoVa is more sensitive to resistive load than assistive load (30). In contrast, both the leading and trailing motors of myoVc took an equal number (~9%) of back steps, suggesting that due to the stiff linkage, both motors are exposed to the resistive load applied by its partner motor. Also, the step lifetimes of the leading and trailing motors of myoVc were not significantly different, although the backward stepping lifetime is three times shorter than that of the leading motor. Interestingly, the delay time analysis with myoVc on actin filaments showed that both leading and trailing motors are affected by the inter-motor distance, suggesting that myoVc is equally sensitive to resistive and assistive loads (Fig. 8, *D* and *F*). In contrast, the delay time analysis of myoVa showed (14) that only the trailing motor coordinates with the leading motor as the inter-motor distance is increased, indicating that there is a differential effect on myoVa heads by the resistive load. We propose that when an ensemble of myoVc motors transports cargo, the motors coordinate with each other and build up strain through their linkage that impacts the stepping dynamics and results in a reduced velocity but longer run length.

Biological implications

MyoVc is associated with secretory granules and is likely involved in their trafficking (4). Transiently formed actin bundles, nucleated by formins at the plasma membrane, are the tracks on which zymogen granules are trafficked prior to secretion in the exocrine pancreas (5). This cellular observation is consistent with the findings here and in Ref. 6, which showed a clear preference of myoVc for actin bundles, such that even teams of myoVc require bundles for continuous motion at physiologic ionic strength. The coordination we show here between myoVc motors in small ensembles is likely to be a mechanism that ensures efficient secretory granule transport in the cell.

Experimental procedures

Protein expression, purification, and actin bundle preparation

Dimeric, constitutively active subfragments of human myoVc (amino acids 1–1105) and mouse myoVa (amino acids 1–1098) were cloned with a SNAP tag at the C terminus followed by a FLAG tag for affinity purification. Each heavy chain contained a biotin tag at the N terminus for attachment of streptavidin Qdots. The biotin tag consisted of 88 residues from the *Escherichia coli* biotin carboxyl carrier protein (31). The heavy chain was co-expressed with a calcium-insensitive calmodulin (CamΔall) (32) to favor complete occupancy of the light chain-binding sites, using the baculovirus/Sf9 cell system as described previously (6, 33, 34). Actin bundles were prepared using actin cross-linked protein fascin as described (16, 33, 35).

Design of DNA origami nanotube

The DNA origami nanotubes were designed as described previously (12, 17). In brief, one or two benzylguanine (SNAP-tag substrate) molecules per myoVa- or myoVc-binding site were attached to the staple strands corresponding to binding sites, *i.e.* columns 1, 13, 25, and 37 on the DNA origami. For imaging purpose, four Cy3 molecules were attached to the DNA, which were located at one end (columns 1–3) of the DNA origami. The folding was conducted by mixing the "base staple mix" containing Cy3-labeled staple strands, the benzylguanine staples, and viral single-stranded DNA (M13mp18 DNA) in TAE Mg^{2+} buffer (40 mM Tris acetate, pH 8.0, 1 mM EDTA and 4 mM $Mg(OAc)_2$). Then, the mixture was heated at 80 °C for 5 min, followed by two-step cooling from 80 to 60 °C. The DNA origami contains 1, 2, or 4 binding sites that are separated by 58 nm. DNA scaffolds were prepared as described previously (7).

Conjugation of motor proteins with a DNA origami nanotube or DNA scaffold

Before conjugation with motor proteins, DNA origami nanotubes were purified with a centrifugal filter device. Briefly, 100 μl of DNA origami nanotubes were transferred to an Amicon Ultra-0.5 filter device (Millipore, 100-kDa MWCO) and washed four times with TAE Mg^{2+} buffer according to the manufacturer's instructions. The concentration of DNA was measured spectrophotometrically at 260 nm. DNA was precipitated by adding 8% (w/v) PEG8000 (MP Biomedicals) in buffer A (25 mM imidazole, pH 7.4, 4 mM $MgCl_2$, 1 mM EGTA, 25 mM KCl, 10 mM DTT) and spun at 15,000 × *g* for 15 min at 22 °C. The precipitated DNA was resuspended in buffer A, mixed with myoVc (or myoVa) at a molar ratio of 5:1 (protein to binding sites), and incubated for 1 h at 27 °C. The unbound motor proteins were removed by passing through ~450 μl of Sephacryl S-500 HR (GE Healthcare) packed in a spin column at 1000 × *g* for 12 s. Conjugation of SNAP-tagged myoVc or myoVa to a double-stranded DNA scaffold was carried out as described (36). The DNA origami-motor complex was diluted to 1 μM myoVc or myoVa motor for experiments.

All DNA origami nanotubes were labeled with Cy3 dyes that were attached to one end of the nanotube. DNA origami containing a single motor was detected from Cy3 or Qdot fluorescence using TIRF microscopy. The streptavidin Qdot (emits at

655 nm) was mixed with myoVa or myoVc at a molar ratio of 4:1 in buffer B (buffer A plus 1 mg/ml BSA) and incubated for 15 min at room temperature. At this molar ratio, ~90% of the Qdots were bound with a single myoVc or myoVa motors calculated using binomial statistics (16). For preparing the 2-motor complex (Fig. 1*A*), we mixed 2 μl of 1 μM streptavidin-conjugated red (emits at 655 nm) and 2 μl of 1 μM green Qdots (emits at 655 nm) into 1 μl of 1 μM myoVa or myoVc (origami-motor complex) in buffer B (buffer A plus 1 mg/ml BSA) and incubated for 15 min at room temperature. Streptavidin-conjugated Qdots were attached specifically to the biotinylated head domain of the motor. A 4-fold molar excess of Qdot over motor was used so that all motors would be labeled with Qdots. If both binding sites on the DNA origami are occupied by motors labeled with Qdots, there will be four equal probabilities: red:red, green:green, red:green, and green:red. Therefore, it is expected that a maximum of 50% of the DNA origamis will be dual color (red and green). We counted the number of Qdot-labeled motors bound to actin filaments and showed that ~40% ($n = 165$) of complexes were labeled with dual color Qdots (Fig. 1*C*). This analysis suggests that the binding affinity of myoVc motors to the origami and labeling with Qdots were both very efficient (80%). Because we have mixed motor to Qdots at a molar ratio of 1:4, it is expected that ~10% of motors would be unlabeled. Therefore, 90% of the binding sites on the origami will be occupied by the motor. The experiments of the 2-motor complex were conducted either at 1 mM MgATP for run length and velocity measurements or at 2 μM MgATP for resolving the individual motor steps.

The efficiency of two motors binding to the origami is very high (90%), and the same trend should persist in the 4-motor case. Based on the statistics for two binding sites on an origami, we calculated using binomial statistics that 65% of the origami will be fully occupied by four motors, and the remaining 35% origami contained either 3, 2, or 1 motor. On average, 3.6 motors were attached to the origami containing four binding sites. DNA origami containing four myoVc motors on actin filament was detected from Qdots. The streptavidin Qdot to myoVc was mixed at a molar ratio of 1:1 so that at least one of four motors were conjugated with Qdot. The myoVc on actin bundle and myoVa on actin filament or bundle were either detected from Cy3 attached to the origami or Qdot (anti-mouse IgG-conjugated Qdots) attached to the origami using Cy3. To visualize Cy3-labeled origami with a Qdot, anti-mouse IgG-conjugated Qdots (Invitrogen; emission 655 nm) were mixed with anti-Cy3 (Sigma) at a molar ratio of 1:3 and incubated for 2 h on ice. A 4-fold molar excess of Qdots was then mixed with the Cy3-labeled origami.

Microscopy and data analysis

In vitro motility experiments were performed at room temperature (23 ± 1 °C) using a TIRF microscope as described previously (37). Experiments were performed in buffer A (25 mM imidazole, pH 7.4, 4 mM $MgCl_2$, 1 mM EGTA, 25 mM KCl, 10 mM DTT) except where noted. Qdots and actin filaments were excited with a 488-nm argon laser. Typically, 1000 images were captured at 10–30 frames/s (1 pixel = 117 nm) using an intensified CCD camera (Stanford Photonics, CA). Qdots were tracked using the SpotTracker 2D or MtrackJ plugins of ImageJ 1.41v to generate motion paths in two dimensions or to measure the total run length (National Institutes of Health, Bethesda, MD) as described (37). Digital images (red and green Qdots) were corrected for color registration error as described (37). Quantum dot-labeled motors were tracked with high spatial and temporal resolution as described previously (33).

Velocity and run length of Qdot-labeled motors were calculated as described previously (37). For step size measurements, experiments were performed at a low ATP concentration (2 μM MgATP). Qdot-labeled motors were tracked using the SpotTracker 2D, which provides *x,y* data of the motion. We then plotted displacement *versus* time trajectories. Using a step-finding program (38), the step sizes and step lifetimes were determined. On actin bundles, step sizes were measured from the average *x,*y values, which were identified using a step-finding program from the time *versus* displacement trajectory. Step sizes were plotted in a histogram and fitted to a Gaussian distribution function and reported as mean ± S.D. The step lifetime of both leading and trailing motors was plotted in a histogram and fitted using the equation $P(t) = tk^2e^{-kt}$, where $1/k$ is the step lifetime (39) and reported as mean ± S.E. of the fit. For statistical significance, a Kruskal-Wallis test with Dunn's multiple comparisons test was performed for run length using GraphPad Prism. The Kolmogorov-Smirnov test with 95% confidence interval was used for the comparison of two sets of run length and step lifetime. For the statistical analysis of multiple sets of velocity data, ANOVA with Bonferroni multiple comparisons test was performed in GraphPad Prism. For statistical significance between two sets of velocity, unpaired *t* test with 95% confidence interval was performed. A p value < 0.05 between two sets of data was considered to be statistically significant. Stepping rate and delay time of motors were measured as a function inter-motor distance as described (14).

Author contributions—M. Y. A. and K. M. T. designed research; M. Y. A., E. B. K., and K. F. performed experiments; M. Y. A., K. M. T., K. F., and K. O. contributed analytical tools; M. Y. A. analyzed data. M. Y. A., K. M. T., and K. F. wrote the article. E. B. K. and K. F. contributed equally to this work. All authors approved the final version of the manuscript.

Acknowledgments—We thank David Warshaw for the use of the TIRF microscope, Thomas Sladewski and Maria Sckolnick for discussion, Andrej Vilfan for insightful comments, and Guy Kennedy for technical assistance.

References

1. Hammer, J. A., 3rd., and Sellers, J. R. (2011) Walking to work: roles for class V myosins as cargo transporters. *Nat. Rev. Mol. Cell Biol.* **13,** 13–26
2. Watanabe, S., Watanabe, T. M., Sato, O., Awata, J., Homma, K., Umeki, N., Higuchi, H., Ikebe, R., and Ikebe, M. (2008) Human myosin Vc is a low duty ratio nonprocessive motor. *J. Biol. Chem.* **283,** 10581–10592
3. Takagi, Y., Yang, Y., Fujiwara, I., Jacobs, D., Cheney, R. E., Sellers, J. R., and Kovács, M. (2008) Human myosin Vc is a low duty ratio, nonprocessive molecular motor. *J. Biol. Chem.* **283,** 8527–8537
4. Jacobs, D. T., Weigert, R., Grode, K. D., Donaldson, J. G., and Cheney, R. E. (2009) Myosin Vc is a molecular motor that functions in secretory granule trafficking. *Mol. Biol. Cell* **20,** 4471–4488

5. Geron, E., Schejter, E. D., and Shilo, B. Z. (2013) Directing exocrine secretory vesicles to the apical membrane by actin cables generated by the formin mDia1. *Proc. Natl. Acad. Sci. U.S.A.* **110,** 10652–10657
6. Sladewski, T. E., Krementsova, E. B., and Trybus, K. M. (2016) Myosin Vc is specialized for transport on a secretory superhighway. *Curr. Biol.* **26,** 2202–2207
7. Gunther, L. K., Furuta, K., Bao, J., Urbanowski, M. K., Kojima, H., White, H. D., and Sakamoto, T. (2014) Coupling of two non-processive myosin 5c dimers enables processive stepping along actin filaments. *Sci. Rep.* **4,** 4907
8. Gross, S. P., Welte, M. A., Block, S. M., and Wieschaus, E. F. (2002) Coordination of opposite-polarity microtubule motors. *J. Cell Biol.* **156,** 715–724
9. Müller, M. J., Klumpp, S., and Lipowsky, R. (2010) Bidirectional transport by molecular motors: enhanced processivity and response to external forces. *Biophys. J.* **98,** 2610–2618
10. Jamison, D. K., Driver, J. W., Rogers, A. R., Constantinou, P. E., and Diehl, M. R. (2010) Two kinesins transport cargo primarily via the action of one motor: implications for intracellular transport. *Biophys. J.* **99,** 2967–2977
11. Larson, A. G., Landahl, E. C., and Rice, S. E. (2009) Mechanism of cooperative behaviour in systems of slow and fast molecular motors. *Phys. Chem. Chem. Phys.* **11,** 4890–4898
12. Bui, H., Onodera, C., Kidwell, C., Tan, Y., Graugnard, E., Kuang, W., Lee, J., Knowlton, W. B., Yurke, B., and Hughes, W. L. (2010) Programmable periodicity of quantum dot arrays with DNA origami nanotubes. *Nano. Lett.* **10,** 3367–3372
13. Derr, N. D., Goodman, B. S., Jungmann, R., Leschziner, A. E., Shih, W. M., and Reck-Peterson, S. L. (2012) Tug-of-war in motor protein ensembles revealed with a programmable DNA origami scaffold. *Science* **338,** 662–665
14. Ali, M. Y., Vilfan, A., Trybus, K. M., and Warshaw, D. M. (2016) Cargo transport by two coupled myosin Va motors on actin filaments and bundles. *Biophys. J.* **111,** 2228–2240
15. Lu, H., Efremov, A. K., Bookwalter, C. S., Krementsova, E. B., Driver, J. W., Trybus, K. M., and Diehl, M. R. (2012) Collective dynamics of elastically coupled myosin V motors. *J. Biol. Chem.* **287,** 27753–27761
16. Ali, M. Y., Previs, S. B., Trybus, K. M., Sweeney, H. L., and Warshaw, D. M. (2013) Myosin VI has a one track mind *versus* myosin Va when moving on actin bundles or at an intersection. *Traffic* **14,** 70–81
17. Torisawa, T., Ichikawa, M., Furuta, A., Saito, K., Oiwa, K., Kojima, H., Toyoshima, Y. Y., and Furuta, K. (2014) Autoinhibition and cooperative activation mechanisms of cytoplasmic dynein. *Nat. Cell Biol.* **16,** 1118–1124
18. Klumpp, S., and Lipowsky, R. (2005) Cooperative cargo transport by several molecular motors. *Proc. Natl. Acad. Sci. U.S.A.* **102,** 17284–17289
19. Rogers, A. R., Driver, J. W., Constantinou, P. E., Kenneth Jamison, D., and Diehl, M. R. (2009) Negative interference dominates collective transport of kinesin motors in the absence of load. *Phys. Chem. Chem. Phys.* **11,** 4882–4889
20. McKenney, R. J., Huynh, W., Tanenbaum, M. E., Bhabha, G., and Vale, R. D. (2014) Activation of cytoplasmic dynein motility by dynactin-cargo adapter complexes. *Science* **345,** 337–341
21. Berger, F., Keller, C., Klumpp, S., and Lipowsky, R. (2012) Distinct transport regimes for two elastically coupled molecular motors. *Phys. Rev. Lett.* **108,** 208101
22. Hill, D. B., Plaza, M. J., Bonin, K., and Holzwarth, G. (2004) Fast vesicle transport in PC12 neurites: velocities and forces. *Eur. Biophys. J.* **33,** 623–632
23. Kural, C., Kim, H., Syed, S., Goshima, G., Gelfand, V. I., and Selvin, P. R. (2005) Kinesin and dynein move a peroxisome *in vivo*: a tug-of-war or coordinated movement? *Science* **308,** 1469–1472
24. Oguchi, Y., Mikhailenko, S. V., Ohki, T., Olivares, A. O., De La Cruz, E. M., and Ishiwata, S. (2010) Robust processivity of myosin V under off-axis loads. *Nat. Chem. Biol.* **6,** 300–305
25. Vershinin, M., Carter, B. C., Razafsky, D. S., King, S. J., and Gross, S. P. (2007) Multiple-motor based transport and its regulation by Tau. *Proc. Natl. Acad. Sci. U.S.A.* **104,** 87–92
26. Schroeder, H. W., 3rd, Mitchell, C., Shuman, H., Holzbaur, E. L., and Goldman, Y. E. (2010) Motor number controls cargo switching at actin-microtubule intersections *in vitro*. *Curr. Biol.* **20,** 687–696
27. Nelson, S. R., Trybus, K. M., and Warshaw, D. M. (2014) Motor coupling through lipid membranes enhances transport velocities for ensembles of myosin Va. *Proc. Natl. Acad. Sci. U.S.A.* **111,** E3986–E3995
28. Driller-Colangelo, A. R., Chau, K. W., Morgan, J. M., and Derr, N. D. (2016) Cargo rigidity affects the sensitivity of dynein ensembles to individual motor pausing. *Cytoskeleton* **73,** 693–702
29. Kad, N. M., Trybus, K. M., and Warshaw, D. M. (2008) Load and P_i control flux through the branched kinetic cycle of myosin V. *J. Biol. Chem.* **283,** 17477–17484
30. Gebhardt, J. C., Clemen, A. E., Jaud, J., and Rief, M. (2006) Myosin-V is a mechanical ratchet. *Proc. Natl. Acad. Sci. U.S.A.* **103,** 8680–8685
31. Cronan, J. E., Jr. (1990) Biotination of proteins *in vivo*. A post-translational modification to label, purify, and study proteins. *J. Biol. Chem.* **265,** 10327–10333
32. Krementsov, D. N., Krementsova, E. B., and Trybus, K. M. (2004) Myosin V: regulation by calcium, calmodulin, and the tail domain. *J. Cell Biol.* **164,** 877–886
33. Ali, M. Y., Krementsova, E. B., Kennedy, G. G., Mahaffy, R., Pollard, T. D., Trybus, K. M., and Warshaw, D. M. (2007) Myosin Va maneuvers through actin intersections and diffuses along microtubules. *Proc. Natl. Acad. Sci. U.S.A.* **104,** 4332–4336
34. Nelson, S. R., Ali, M. Y., and Warshaw, D. M. (2011) Quantum dot labeling strategies to characterize single-molecular motors. *Methods Mol. Biol.* **778,** 111–121
35. Hodges, A. R., Bookwalter, C. S., Krementsova, E. B., and Trybus, K. M. (2009) A nonprocessive class V myosin drives cargo processively when a kinesin-related protein is a passenger. *Curr. Biol.* **19,** 2121–2125
36. Furuta, K., Furuta, A., Toyoshima, Y. Y., Amino, M., Oiwa, K., and Kojima, H. (2013) Measuring collective transport by defined numbers of processive and nonprocessive kinesin motors. *Proc. Natl. Acad. Sci. U.S.A.* **110,** 501–506
37. Ali, M. Y., Kennedy, G. G., Safer, D., Trybus, K. M., Sweeney, H. L., and Warshaw, D. M. (2011) Myosin Va and myosin VI coordinate their steps while engaged in an *in vitro* tug of war during cargo transport. *Proc. Natl. Acad. Sci. U.S.A.* **108,** E535–E541
38. Kerssemakers, J. W., Munteanu, E. L., Laan, L., Noetzel, T. L., Janson, M. E., and Dogterom, M. (2006) Assembly dynamics of microtubules at molecular resolution. *Nature* **442,** 709–712
39. Yildiz, A., Forkey, J. N., McKinney, S. A., Ha, T., Goldman, Y. E., and Selvin, P. R. (2003) Myosin V walks hand-over-hand: single fluorophore imaging with 1.5-nm localization. *Science* **300,** 2061–2065